UC Irvine
UC Irvine Previously Published Works

Title
Propagating and evanescent edge diffracted waves for a semi-infinite periodic dipole array

Permalink
https://escholarship.org/uc/item/1vj534wm

ISBN
9780780344785

Authors
Capolino, F
Albani, M
Maci, S
et al.

Publication Date
1998

DOI
10.1109/aps.1998.699103

Copyright Information
This work is made available under the terms of a Creative Commons Attribution License, availalbe at https://creativecommons.org/licenses/by/4.0/

Peer reviewed

eScholarship.org Powered by the California Digital Library
University of California

PROPAGATING AND EVANESCENT EDGE DIFFRACTED WAVES FOR A SEMI-INFINITE PERIODIC DIPOLE ARRAY

F. CAPOLINO[1], M. ALBANI[1], S. MACI[1], L. B. FELSEN[2]

[1]*Dept. of Information Engineering, University of Siena, Via Roma 56, 53100, Siena, Italy.*
[2]*Dept. of Aerospace and Mechanical Engineering and Dept. of Electrical and Computer Engineering, Boston University, 110 Cummington Street, Boston, MA 02215, USA.*

1. INTRODUCTION

The electromagnetic modeling of large finite array antennas may be carried out by using a Floquet Wave (FW) representation of the infinite array Green's function. To account for array edge effects, this representation needs to be modified as described in [1]; in particular, the Green's function of a finite array is collectively represented as the radiation from a superposition of continuous truncated FW distributions over the array aperture. Since the FW series exhibits excellent convergence properties when the observation point is located away from the array surface, this representation is found to be more efficient than the direct summation of the spatial contributions from each element of the array, especially when each FW aperture distribution is treated asymptotically. Furthermore, the collective approach provides basic physical insight into the relevant scattering mechanisms for this class of problems. By invoking the locality of high-frequency phenomena as formalized in the Geometrical Theory of Diffraction (GTD), an actual rectangular array may be treated by accounting for local canonical edge and corner effects [2].

In order to understand and quantify the high-frequency wave processes associated with FW edge diffraction, this paper deals with the canonical Green's function of a semi-infinite phased array of dipoles in free space. The diffracted field contributions due to each incident FW field are cast in a dyadic form that highlights the behavior of TE and TM waves. Special attention is given to evanescent diffracted fields, which are associated with high order FWs.

2. FORMULATION

The geometry of a phased array of dipoles oriented along the direction $\bar{J}_0 = J_{0x}\hat{x} + J_{0z}\hat{z}$ is shown in Fig. 1, with definition of both cartesian and cylindrical coordinates; here and in the following a caret denotes a unit vector and an overbar a general vector. Referring to Fig. 1, d_x and d_z are the interelement periods in the x and z directions, respectively. The dipoles are linearly phased, with γ_x and γ_z denoting the element-to-element phase shift along the x and z coordinates, respectively. With a suppressed time dependence $\exp(j\omega t)$, the dipole currents can be represented as

$$\bar{J}_{nm} = \bar{J}_0 \, e^{-j\bar{\gamma}\cdot\bar{d}_{nm}} \qquad (1)$$

where $\bar{\gamma} \equiv \gamma_x\hat{x} + \gamma_z\hat{z}$ and $\bar{d}_{nm} \equiv nd_x\hat{x} + md_z\hat{z}$ is the position of (n,m)-th dipole. TM_z and TE_z fields are calculated via the magnetic and

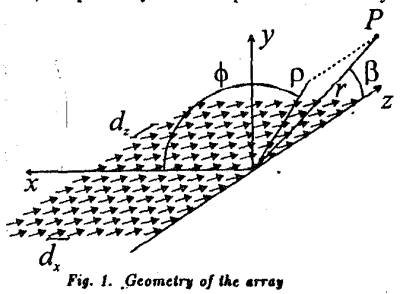

Fig. 1. Geometry of the array

0-7803-4478-2/98/$10.00 © 1998 IEEE

electric Hertz potentials $\Pi' \hat{z}$ and $\Pi'' \hat{z}$, respectively [3]. By summing the potentials due to all sources in their spectral representation, it is straightforward to obtain the z-component of the electric and magnetic fields at $\bar{r}$ as

$$\begin{bmatrix} E_z(\bar{r}) \\ \zeta H_z(\bar{r}) \end{bmatrix} = \frac{\zeta}{8\pi^2} \sum_{m=-\infty}^{\infty} \sum_{n=0}^{\infty} e^{-j\bar{\gamma}\cdot\bar{d}_{nm}} \int_{-\infty}^{\infty}\int_{-\infty}^{\infty} \bar{\bar{D}}(k_x,k_y,k_z)\cdot\bar{J}_{nm} e^{-j\bar{k}\cdot(\bar{r}-\bar{d}_{nm})} dk_z dk_x \quad (2)$$

Here, $\bar{\bar{D}} = D_{ij}$ $(i,j=1,2)$ with $D_{11}=\frac{k_x k_z}{k k_y}$, $D_{12}=\frac{k_z^2-k^2}{k k_y}$, $D_{21}=1$, $D_{22}=0$, and $\bar{k} = k_x\hat{x} + k_y\hat{y} + k_z\hat{z}$.

The branch of $k_y=\sqrt{k^2-k_x^2-k_z^2}$ is chosen to render $\Im m(yk_y)<0$ on the top Riemann sheet of the complex k_x-plane, for real k_z. The transverse component E_x and E_y can be determined by differentiating the E_z and H_z fields. From (2) we note that while dipoles oriented along z generate only TM_z waves, dipoles oriented along x generate both TE_z and TM_z waves. Interchanging the sequence of the semi-infinite n-sum and spectral integration operations, the resulting n-series can be calculated in closed form. Next, applying the Poisson summation formula to the bilaterally infinite m-series and the (k_x, k_z) spectral integration operations, we obtain

$$\begin{bmatrix} E_z(\bar{r}) \\ \zeta H_z(\bar{r}) \end{bmatrix} = \frac{\zeta}{4\pi d_z} \sum_{q=-\infty}^{\infty} \int_{-\infty}^{\infty} \frac{\bar{\bar{D}}(k_{xp},k_{ypq},k_{zq})\cdot\bar{J}_0}{1-e^{jd_x(k_x-\gamma_x)}} e^{-j\bar{k}\cdot\bar{r}} dk_z \quad (3)$$

in which $k_{yq}=\sqrt{k^2-k_x^2-k_{zq}^2}$, whereas $k_{zq}=\gamma_z+2\pi q/d_z$ and the real poles located at $k_{xp}=\gamma_x+2\pi p/d_x$ (which are avoided by clockwise indentation of the integration path) are the FW propagation constants in the z and x directions, respectively.

3. HIGH-FREQUENCY SOLUTION

In order to evaluate each integral in (3), the contour is deformed into the steepest descent path (SDP) through its relevant saddle point. The poles captured in this deformation give rise to residue contributions. Thus, the integral in (5) is reduced to

$$\begin{bmatrix} E_z(\bar{r}) \\ \zeta H_z(\bar{r}) \end{bmatrix} = \sum_{p=-\infty}^{\infty} \sum_{q=-\infty}^{\infty} \begin{bmatrix} E_z(\bar{r}) \\ \zeta H_z(\bar{r}) \end{bmatrix}_{pq}^{FW} + \sum_{q=-\infty}^{\infty} \begin{bmatrix} E_z(\bar{r}) \\ \zeta H_z(\bar{r}) \end{bmatrix}_{q}^{D} \quad (4)$$

$$\begin{bmatrix} E_z(\bar{r}) \\ \zeta H_z(\bar{r}) \end{bmatrix}_{pq}^{FW} = \frac{\zeta}{2d_x d_z} \bar{\bar{D}}(k_{xp},k_{ypq},k_{zq})\cdot\bar{J}_0\, e^{-j\bar{k}_{pq}\cdot\bar{r}} U(\cos\phi-\cos\phi_{pq}^{SB}) \quad (5)$$

$$\begin{bmatrix} E_z(\bar{r}) \\ \zeta H_z(\bar{r}) \end{bmatrix}_{q}^{D} \sim \frac{j\zeta}{2d_z} \left\{ \frac{k_{ypq}\bar{\bar{D}}(k_{\rho p}\cos\phi, k_{\rho p}\sin\phi, k_{zq})}{1-e^{-jd_x(k_{pq}-\gamma_x)}} - \frac{1}{2jd_x} \sum_{p=-P}^{P} \left(\bar{\bar{D}}(k_{xp},k_{ypq},k_{zq}) \right.\right.$$

$$\left.\left. \frac{F(\delta_{pq-}^2)-1}{\sin\left(\frac{\phi-\phi_{pq}}{2}\right)} + \mathrm{sgn}(k_{xp})\bar{\bar{D}}(k_{xp},-k_{ypq},k_{zq}) \frac{F(\delta_{pq+}^2)-1}{\sin\left(\frac{\phi+\phi_{pq}}{2}\right)} \right) \right\} \cdot \bar{J}_0 \frac{e^{-j(k_{pq}\rho+k_{zq}z)}}{\sqrt{2j\pi k_{pq}\rho}} \quad (6)$$

The expression in (5) (with $U(\alpha)=1$ for $\alpha>0$ or $U(\alpha)=0$ for $\alpha<0$) arises from residues, whereas (6) arises from the high frequency uniform asymptotic evaluation, via the Van der Waerden method [3], of the SDP integral. In (5)

and (6), $\bar{k}_{pq}=k_{xp}\hat{x}+k_{ypq}\hat{y}+k_{xq}\hat{z}$ is the wavevector of the pq-th FW, and

$$k_{pq}=\sqrt{k^2-k_{xq}^2} \quad \text{and} \quad k_{ypq}=\sqrt{k^2-k_{xp}^2-k_{xq}^2} \tag{7}$$

with the branches of the square roots defined so that $\Im m(k_{pq})<0$ for $|k_{xq}|>k$, and $\Im m(yk_{ypq})<0$ when $k_{xp}^2+k_{xq}^2>k^2$. Furthermore, Q denotes the number of poles extracted and F represents the standard Fresnel-type transition function of the Uniform Theory of Diffraction (UTD) with argument $\delta_{pq\pm}=\sqrt{2k_{\rho q}\rho}\sin[(\phi\pm\phi_{pq})/2]$. The two contributions defined in (5) and (6) are discussed next.

3.1. FWs contributions

Except for the Heaviside unit step function U that bounds their domain of existence at the shadow boundary planes $\phi=\phi_{pq}^{SB}$, the residue contributions (5) represent the FWs of the doubly infinite array of dipoles. In particular, it can be seen that $\phi_{pq}^{SB}=\Re e(\phi_{pq})-\tan^{-1}(\sinh(\Im m(\phi_{pq}))$ for $|k_{xq}|\leq k$ while $\phi_{pq}^{SB}=\pi/2$ for $|k_{xq}|>k$, where $\phi_{pq}=\cos^{-1}(k_{xp}/k_{pq})$ specifies the direction of the azimuthal component of the FW wavevector. . Poles with $k_{xp}^2+k_{zq}^2<k^2$ are associated with propagating Floquet waves (PFWs) but all the others with evanescent Floquet waves (EFWs). The PFWs are homogeneous plane waves that propagate in the $\bar{k}_{pq}$ direction with the speed of light. For them the shadow boundary angle coincides with the angle of propagation in the azimuthal plane ($\phi_{pq}^{SB}=\phi_{pq}$). The EFWs are inhomogeneous plane waves that propagate slowly (w.r.t. the speed of light) in the direction $k_{xp}\hat{x}+k_{xq}\hat{z}$ and decay exponentially in the $\pm\hat{y}$ direction away from the array plane. The transition between the homogeneous and evanescent FWs is defined by the cut-off condition $k_{ypq}=0$. Owing to the EFWs exponential decay along $|y|$, the convergence of the first series in (4) is very rapid when the observation point is located sufficiently far away from the array surface.

3.2. Evanescent and propagating diffracted waves

The uniform saddle point evaluation of (3) provides diffracted FW field contributions emanating from the edge of the array. The function F in (6) is discontinuous when its complex argument crosses the positive imaginary axis, which occurs exactly at the shadow boundary angle defined earlier. The diffracted field contributions smoothly compensate for the discontinuity of the FWs at the shadow boundary. Each pq-th FW diffracts at a point Q_q on the array edge according to a generalized Fermat principle that may be expressed as

$$k\,\frac{(\bar{r}-\bar{z}_q)}{|\bar{r}-\bar{z}_q|}\cdot\hat{z}=\bar{k}_{pq}\cdot\hat{z} \tag{8}$$

where $\bar{z}_q$ denotes the p-independent location of Q_q. Therefore, the diffracted field contribution has been tagged with only a single summation index q. Diffracted rays produced by FWs with different axial component k_{zq} arise from distinct diffraction points Q_q (one for each q). For $|k_{xq}|<k$, all diffracted rays emanating from these points lie on a diffraction cone with aperture semi-angle $\beta_q=\cos^{-1}(k_{xq}/k)$, which becomes more acute with decreasing FW phase velocity along z. When $|k_{xq}|\to k$, the diffraction cone collapses onto the z-axis; for $|k_{xq}|>k$, there is no real point Q_q on the edge satisfying (8), and β_q becomes complex, as do the diffracted rays. The resulting diffracted field is evanescent along the ρ direction, with exponential decay term $\exp(-|k_{pq}|\rho)$. This yields rapid convergence for diffracted ray series in (4), sufficiently far from the edge. The diffracted FWs which contribute substantially to the scattered field are generated by all PFWs, and those EFWs for which $|k_{xq}|<k$.

4. ILLUSTRATIVE EXAMPLE

Numerical calculations have been carried out to test the accuracy and effectiveness of the asymptotic solution (3), as well as to highlight the effects of the cut-off transition. A reference solution for a strip array along x is constructed via element-by-element summation of individual source contributions over a square array with $m \leq M=2000$ and $n \leq N=100$. The m-dimension permits neglecting the truncation effects along z. The dipoles are tilted 45° with respect to z. In Fig. 2, with λ being the wavelength, the near field scan is at a radial distance $\rho=2.2\lambda$ from the z-axis in the $z=0$ (*i.e.* $m=0$) plane; $d_x=0.5\lambda$, $d_z=1.1\lambda$, $\gamma_x'=-0.945\lambda^{-1}$ and $\gamma_z'=0.5\lambda^{-1}$. The $\hat{z}$ and $\hat{\phi}$ electric field components are shown along the scan. The solid curve is obtained by the high-frequency solution (4), including diffracted fields from both edges. These curves coincide with the reference solutions (circles). Additionally, dashed curves are presented, that are obtained by neglecting the diffracted field contributions. The geometrical configuration is such that $\bar{E}^{FW}_{0-1}$, $\bar{E}^{FW}_{00}$ are propagating, while $\bar{E}^{FW}_{01}$ is evanescent, but close to its cut-off condition. The three corresponding diffracted fields $\bar{E}^{d}_{-1}$, $\bar{E}^{d}_{0}$, and $\bar{E}^{d}_{1}$ all propagate away from the edge. Higher order FW and their pertinent diffracted fields are neglected due to their strong exponential decay along y and ρ, respectively. It is evident that the diffracted field contributions strongly affect the accuracy of the prediction, especially that relevant to the close-to-cut-off EFW. It is worth noting that even in this critical regime, the field predicted by (4) is in excellent agreement with respect to the reference solution, and the diffracted field (6) well compensates for the discontinuity of the EFW.

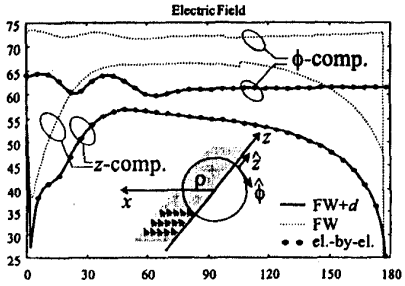

Fig. 2. Electric field at $\rho=2.2\lambda$ from the edge of a 2000×100 array of 45° tilted dipoles.

REFERENCES

[1] L. Felsen, L. Carin, "Diffraction Theory of Frequency and Time Domain Scattering by Weakly aperiodic Truncated thin Wire Gratings", *Journ. Opt. Soc. Am.*, Feb.1994.

[2] F. Capolino, M. Albani, A. Neto, S. Maci, L. B. Felsen "Vertex-diffracted Floquet waves at a corner array of dipoles", Intern. Conf. on Electromag. in Advanced Applicat. (ICEAA), Torino, Sept. 16-18, 1997.

[3] L.B. Felsen, N. Marcuvitz, *Radiation and Scattering of Waves,* IEEE Press, Piscataway, New Jersey 1994.